ROYAL SOCIETY OF CHEMISTRY

PAPER

Check for updates

Direct and selective nanosensor for amyloid-β oligomers in serum for Alzheimer's disease diagnosis†

Qingting Song,[a] Hailong Zhang,[b] Yue Lan,[b] Jia Kong,[b] Man Shing Wong [ID] *[b] and Hung-Wing Li [ID] *[a]

The rising prevalence of Alzheimer's disease (AD) highlights an urgent need for ultra-sensitive diagnostic tools that facilitate early detection and intervention. Soluble Aβ oligomers (AβOs) have emerged as a key focus due to their specificity for AD pathology. This study introduces a magnetic nanoplatform-based ultrasensitive diagnostic assay for AβO detection, utilizing a novel custom-designed AβO-selective fluorophore, named O-SLM. This innovative approach achieves a sensitivity nearly tenfold greater than that of a comparative ELISA kit, with a detection limit as low as 25 fM. The assay requires minimal sample volumes and streamlines the protocol by omitting detection antibodies. It effectively distinguishes AD patients from healthy individuals through serum AβO quantification, demonstrating the versatility of our ultra-sensitive assay across various biomarkers.

1. Introduction

Alzheimer's disease (AD) currently affects millions globally, with prevalence expected to increase significantly as populations age, imposing substantial social and economic burdens on healthcare systems.[1] The severity of AD is underscored by its profound effects on quality of life and societal inclusion. A recent report revealed that 88% of individuals living with dementia faced discrimination in 2024, up from 83% in 2019.[2] This stigma, coupled with the progressive nature of the disease, emphasizes the urgent need for enhanced treatment and diagnostic strategies.

Current AD treatments primarily focus on symptom management rather than addressing the underlying pathology. Approved drugs, such as cholinesterase inhibitors and NMDA receptor antagonists, provide limited cognitive benefits but do not halt or reverse disease progression. Recent advancements in monoclonal antibodies targeting amyloid-beta (Aβ), including aducanumab and lecanemab, show potential in reducing amyloid plaques; however, their clinical efficacy remains limited and controversial due to high costs, side effects, and modest cognitive improvements.[3,4] The progressive nature of AD necessitates early diagnostic methods, as significant neuronal damage occurs long before clinical symptoms

manifest. Early intervention could enhance the effectiveness of emerging therapies by targeting the disease at a stage when neuronal loss is minimal, allowing patients and families to plan for future care and participate in clinical trials.[5]

The amyloid cascade hypothesis has long been a foundational framework for understanding AD pathogenesis for over 25 years.[6] This hypothesis asserts that the accumulation and deposition of Aβ peptides in the brain are the primary drivers of AD pathology.[7] However, recent research has shifted focus from Aβ plaques to soluble Aβ oligomers as critical neurotoxic agents in AD progression.[3] AβO plays a crucial role in refining the amyloid cascade hypothesis. These soluble aggregates are believed to directly damage synapses, activate microglia, and initiate a cascade of pathological events leading to neurodegeneration.[3,6] Unlike Aβ plaques, oligomers correlate more closely with cognitive decline and are considered primary mediators of synaptic dysfunction in AD.[8] This evolving understanding has spurred the development of novel therapeutic approaches targeting AβOs, as well as new biomarkers for AD.

Blood-based protein biomarkers have emerged as promising tools for diagnosing AD, offering a less invasive and potentially more accessible alternative to traditional methods. Among key biomarkers, including Aβ monomer, tau, phosphorylated tau (p-tau), and neurofilament light chain (NfL),[9,10] AβOs demonstrate superior diagnostic potential.[4] Research indicates that AβOs accumulate in cerebrospinal fluid (CSF) in an AD-dependent manner, suggesting their utility as early indicators of disease progression.[11] Their presence in blood, albeit at lower concentrations, opens avenues for minimally invasive screening.[12] While other biomarkers such as tau and NfL

[a] *Department of Chemistry, The Chinese University of Hong Kong, Sha Tin, Hong Kong SAR, China. E-mail: hungwingli@cuhk.edu.hk*

[b] *Department of Chemistry, Hong Kong Baptist University, Kowloon Tong, Hong Kong SAR, China*

provide complementary information, AβOs stand out due to their specificity to AD pathology and potential for early detection, making them a critical focus for developing ultrasensitive diagnostic assays.[13,14]

Current diagnostic tools for AβOs in AD are evolving rapidly, with promising advancements in both sensitivity and specificity. One notable approach involves antibody-based detection methods such as ACU193, which has demonstrated high specificity for Aβ oligomers bound to primary neurons.[15] This technique offers potential applications in both therapeutic and diagnostic settings. Additionally, the development of novel fluorescent probes like quinoline-derived half-curcumin-dioxaborine (Q-OB) shows potential for early-onset AD diagnosis by targeting AβOs.[14,16] As research progresses, the focus remains on developing tools that can reliably detect AβOs at presymptomatic stages, potentially revolutionizing AD diagnosis and treatment monitoring. Current methods often struggle with the low concentrations of oligomers in peripheral fluids, necessitating ultra-sensitive detection techniques.

We previously reported an ultra-sensitive assay based on magnetic nanoparticles for detecting neurofilament light chain protein (NfL).[17] In this study, we have adapted this direct ultra-sensitive assay for the detection of AβO to fulfill the critical need for early diagnosis of AD (Scheme 1). Specifically, magnetic nanoparticles were functionalized with the Oligomer A11 polyclonal antibody to form magnetic nanoprobes (A11-Fe$_3$O$_4$@SiO$_2$ NPs). After capturing AβO, the custom-designed fluorophore O-SLM which is selective AβO over monomeric Aβ, was employed for signal amplification. The use of magnetic nanoparticles facilitates the isolation and preconcentration of target proteins,

while the immune interaction between the A11 antibody and AβO, combined with effective signal amplification from O-SLM, enhances overall assay sensitivity. This combined approach achieves a sensitivity nearly tenfold greater than a commercial ELISA kit, with a detection limit of 25 fM. The assay effectively differentiates AD patients from healthy individuals through serum AβO quantification, demonstrating its versatility across various biomarkers.

2. Experimental

2.1 Reagents

Fe$_3$O$_4$ nanoparticles (10–30 nm, 25%) were obtained from RuixiBiotech (Xi'an, China). Glutaraldehyde (GA, 70%), (3-Aminopropyl)triethoxysilane (APTES), and tetraethyl orthosilicate (TEOS) were obtained from Sigma (USA). Oligomer A11 polyclonal antibody and human amyloid-β oligomers (AβO) were purchased from Thermo Fisher Scientific (USA). 4G8 β-amyloid antibody was purchased from Biolegend (USA). The human serum samples were purchased from BioIVT (USA). All other chemicals were of analytical grade and obtained from Sigma (USA).

2.2 Characterization

The transmission electron microscopy (TEM) images of the NPs were recorded on an FEI Tecnai Spirit 12 microscope (Japan). Hydrodynamic diameters and zeta potentials were determined by Malvern Mastersizer 2000, Zetasizer Nano ZS90 (UK). The fluorescence intensity was measured by a spectrofluorometer (Edinburgh instruments FS5).
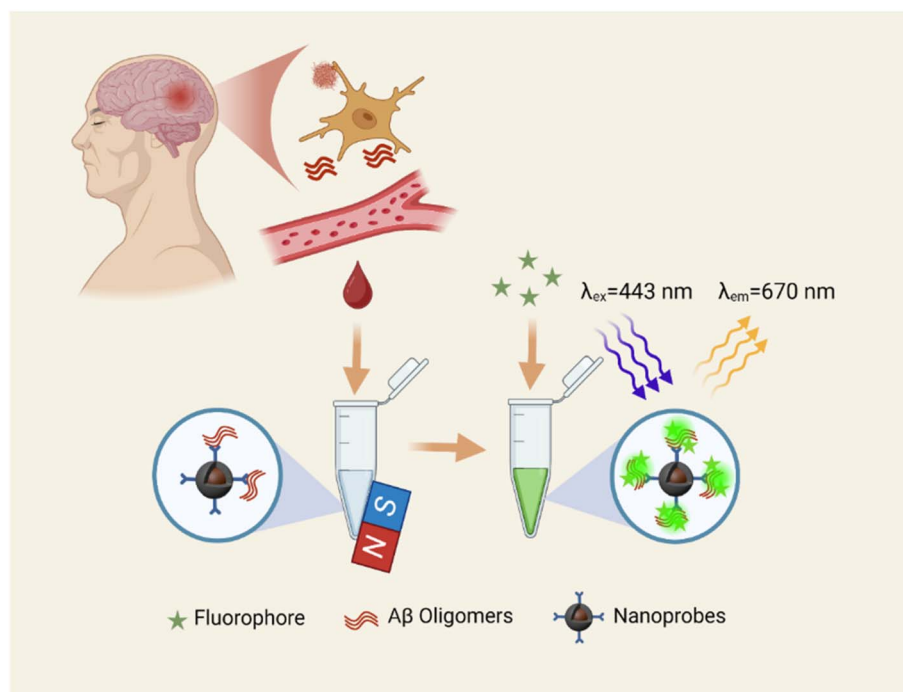
Scheme 1 Schematic illustration of employing capture antibody-modified magnetic nanoparticles (A11-Fe$_3$O$_4$@SiO$_2$) to detect Aβ oligomers using fluorescence analysis.

2.3 Fabrication of silica-coated iron oxide nanoparticles ($Fe_3O_4@SiO_2$ NPs)

The $Fe_3O_4@SiO_2$ NPs were synthesized as reported.[17] Briefly, a mixture of 5 mL of 28% NH_4OH solution, 29 mL of distilled water, 27.5 mL of ethanol, and 1 mL of 40 mg mL^{-1} Fe_3O_4 NPs was prepared by mechanically stirring. Then, 1/15 (v/v) of TEOS diluted in ethanol was added dropwise to the stirred solution and continuously stirred for up to five hours. Lastly, the nanoparticles were resuspended in 10 mL ethanol after washing with distilled water and ethanol for three times, respectively.

2.4 Construction of nanoprobes

The capture antibody, A11, was coupled to $Fe_3O_4@SiO_2$ NPs using the crosslinker glutaraldehyde. 10 mg $Fe_3O_4@SiO_2$ NPs were combined with 1.5 mL APTES and 3 mL ethanol solution, followed by stirring at 73 °C for 24 h. The resulting nanoparticles were washed twice with ethanol and subsequently with water, after which they were redispersed in deionized water. The NPs were then functionalized with 250 μL of GA and vortexed at room temperature for 2.5 hours. Following this, the nanoparticles underwent multiple washes with water to remove any unreacted glutaraldehyde and were redispersed in PBS (pH7.4, 10 mM). Finally, the synthesized nanoparticles were incubated with A11 polyclonal antibody for 1.5 hours. The formed magnetic nanoprobes were isolated from the solution using a magnet, washed twice and then redispersed in 500 μL of PBS.

2.5 Optimization of the conditions for the nanosensor

A series of experiments was systematically conducted to find the optimal condition by varying a single parameter at a time, and the performance was assessed by comparing the fluorescence intensity of the fluorophore at its maximum emission wavelength of 670 nm. To evaluate the suitable reaction temperature, the entire process was conducted at room temperature (25 °C) or human temperature (37 °C). To determine the optimal coverage of A11 on the NPs, concentrations of 100, 300, 600, and 900 nM of A11 were introduced for conjugation with the NPs, resulting in the synthesis of nanoprobes with varying A11 densities on their surfaces. Subsequently, to optimize the concentration of the nanoprobes suitable for the detection assay, various concentrations of 1, 2, and 3 mg mL^{-1} were used to incubate with the target analytes to form immunocomplexes. Optimal incubation period was evaluated by incubating the nanoprobes with analytes for 30, 60, and 90 minutes. In addition, to determine the optimal concentration of the turn-on fluorophore needed for effective labeling, the immunocomplexes were incubated with the fluorophore at different concentrations of 30, 40, and 50 μM. Next, to determine the optimal concentration of the detection antibody (4G8) in this protocol, 4G8 concentrations of 0.6, 6, and 60 nM were tested. Finally, to check whether the detection methodology can be simplified by skipping the secondary antibody, a comparative evaluation was performed through co-incubation of the nanoprobes and the targets both with and without 4G8.

2.6 Quantification of the analytes

The detection condition chosen represents the optimal outcome of the optimization experiments. Calibration curve method was utilized to quantify the interested protein biomarkers in serum samples. For detail, specific concentrations of AβO were incubated with 2 mg mL^{-1} magnetic nanoprobes, which were prepared by conjugating $Fe_3O_4@SiO_2$ NPs with 600 nM A11 for 60 minutes at 25 °C to yield immunocomplexes. Then magnetic separation was undertaken to isolate the resulting magnetic immunocomplexes, which were then washed with PBS. Next, O-SLM at concentration of 40 μM was added to label the immunocomplexes. Fluorescence measurements were taken after a brief 10 minutes incubation using the spectrofluorometer, with the fluorescent signal at 670 nm recorded for constructing an external calibration curve.

Human serum was initially diluted 10-fold with PBS (10 mM, pH 7.4) and the AβO levels in serum samples was determined by using the calibration curve method.

2.7 Selectivity of the nanosensor

To assess the selectivity, nanoprobes were incubated with 500 fM of Aβ40 monomer, 500 fM of Aβ42 monomer, 500 fM of AβO, and a mixture of all three species under optimized conditions, respectively. The formed complexes were subsequently labeled with 40 μM of O-SLM. The fluorescence intensities recorded at 670 nm were compared to evaluate the selectivity.

3. Results and discussion

3.1 Design and synthesis

The $Fe_3O_4@SiO_2$ NPs were fabricated by sol–gel reaction, followed by the preparation of the nanoprobes through the conjugation of APTES-activated $Fe_3O_4@SiO_2$ with the polyclonal capture antibody (A11) utilizing a crosslinker, glutaraldehyde (GA) (Fig. S1†). As illustrated in Fig. 1a, the morphology of the $Fe_3O_4@SiO_2$ is spherical, with the size distribution indicating an average diameter of ~71.0 ± 8.2 nm. Dynamic light scattering (DLS) analysis demonstrates that the $Fe_3O_4@SiO_2$ NPs possess a hydrodynamic size of ~95 nm in aqueous solution with a polydispersity index value of 0.113, suggesting uniform dispersion of the NPs in aqueous media (Fig. 1b). The preparation process of nanoprobes was monitored through changes in surface charge. As depicted in Fig. 1c, the zeta potential of bare $Fe_3O_4@SiO_2$ in pH 7.4 PBS buffer is highly negative, whereas it becomes positive following APTES modification due to the introduction of amino groups on the surface. Subsequently, the surface charge exhibits a slight positive shift after GA activation, presenting aldehyde groups on the surface. Following A11 immobilization, the surface charges of the nanoprobes shift negatively from 36.5 mV to 15.9 mV, indicating the successful preparation of the nanoprobes. The nanoprobes also exhibit favorable magnetic properties (Fig. S2†), being attracted to the magnet side within 30 seconds, which facilitates efficient sample manipulation using a magnet bar. The magnetic nanoprobes were incubated with AβO and the detection antibody sequentially to form magnetic
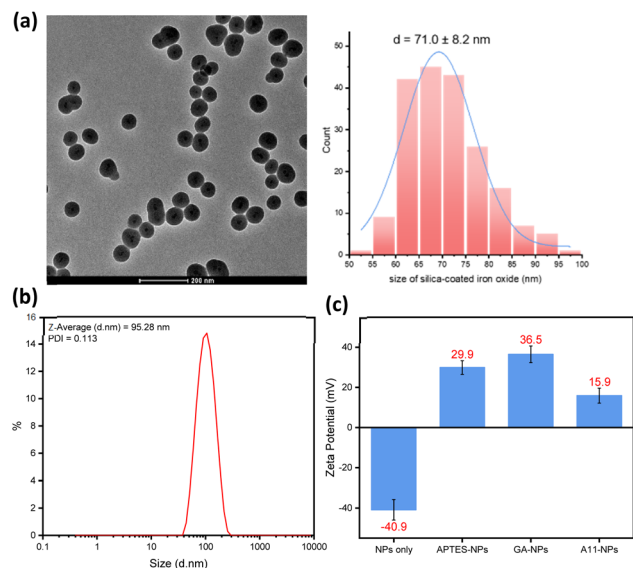
Fig. 1 (a) Transmission electron microscopy (TEM) image and size distribution of $Fe_3O_4@SiO_2$ NPs. (b) Hydrodynamic size of $Fe_3O_4@SiO_2$ NPs. (c) Zeta potential of the bare $Fe_3O_4@SiO_2$ NPs (NPs only), APTES-modified $Fe_3O_4@SiO_2$ NPs (APTES-NPs), GA-activated $Fe_3O_4@SiO_2$ NPs (GA-NPs), and capture antibody conjugated $Fe_3O_4@SiO_2$ NPs (A11-NPs).

immunocomplexes, which were subsequently labelled with the custom-designed turn-on fluorophore, O-SLM, after rinsing and preconcentrating. The fluorescence enhancement was measured to quantify the concentration of the target protein in the test sample.

O-SLM (Fig. 2a) is a tailored turn-on fluorophore featuring a carbazole-derived cyanine structure that exhibits significant fluorescence enhancement upon binding to AβO. The synthesis and structural characterization of O-SLM are detailed in the ESI† (Scheme S1 and Fig. S3). Given that real serum is a highly complex matrix containing a diverse array of proteins that could potentially interfere with the assay, we evaluated the selectivity of O-SLM against various biologically relevant proteins, including Aβ42 species (monomers, oligomers, and fibrils), BSA, Tau-441 monomer, α-Synuclein, islet amyloid polypeptide (IAPP), and human serum albumin (HSA). As shown in Fig. 2b, O-SLM did not exhibit significant fluorescence enhancement with most of these proteins but showed a pronounced fluorescence enhancement specifically with Aβ oligomers and fibrils, underscoring its desirable interactions and strong selectivity. To further investigate O-SLM's binding affinity for these two forms, their molar ratios relative to O-SLM were increased. As illustrated in Fig. 2c, the fluorescence intensities of O-SLM in the presence of Aβ fibrils and Aβ oligomers were comparable at high concentrations of these proteins, suggesting that O-SLM's selectivity between Aβ fibrils and oligomers diminishes under these conditions. To elucidate the binding mechanism of O-SLM with Aβ oligomers, molecular docking simulations were conducted using AutoDock Vina program (Fig. S4†). A strong interaction between O-SLM and an Aβ42 oligomer was predicted with a binding score of -4.406 kcal mol^{-1}, which was attributed
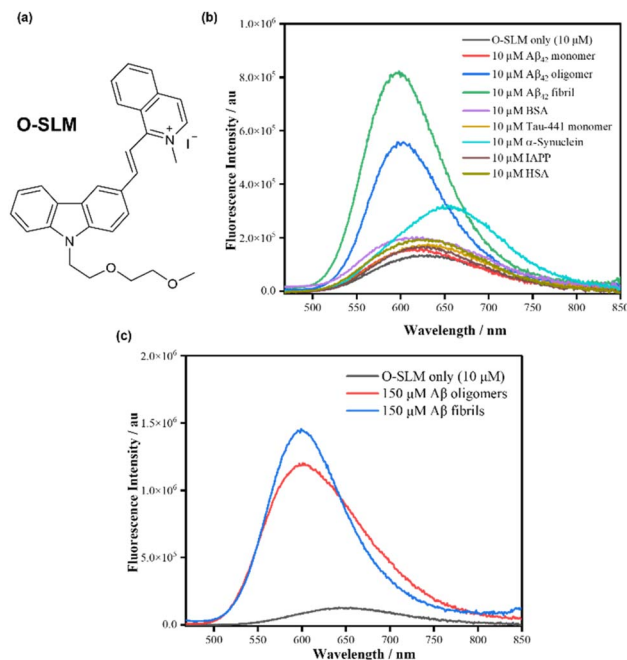

Fig. 2 (a) Chemical structure of the fluorophore, O-SLM. (b) Fluorescence intensity of O-SLM (10 μM) in the presence of 10 μM of Aβ42 species (monomers, oligomers and fibrils), BSA, Tau-441 monomer, α-synuclein, IAPP and HSA measured in 25 mM phosphate buffer (pH = 7.4) at 443 nm, respectively. (c) Fluorescence intensity of O-SLM (10 μM) in the presence of 150 μM Aβ fibrils and Aβ oligomers measured in 25 mM phosphate buffer (pH = 7.4) at 443 nm, respectively.

to π-cation/anion and hydrogen bonds (involving Arg5, Asp7) as well as π-alkyl interactions (involving Phe4, Arg5, His6) between O-SLM and the Aβ42 oligomer.

Moreover, amyloid fibrils are rarely detected in serum due to their larger size and lower solubility, leading to their accumulation primarily in brain tissue rather than circulation in the bloodstream. In contrast, monomeric and oligomeric forms are more commonly found in serum. Therefore, O-SLM demonstrates significant potential for specifically detecting Aβ oligomers in serum samples, which are critical biomarkers for early-stage Alzheimer's disease.

3.2 Optimization of the immunoassay

Accurate quantification of the interested biomarkers, which are often found only in trace amounts in the body fluids of AD patients—particularly in the early stages—critically depends on the sensitivity of the detection assay. To improve the assay performance, optimization was performed to achieve the optimal conditions. The initial step involved assessing the appropriate reaction temperature by conducting the entire process at either room temperature (25 °C) or physiological temperature (37 °C). As illustrated in Fig. 3a, room temperature proved more conducive to assay performance.

To maximize target capture efficiency, we optimized the coverage of the capture antibodies (A11) on the NPs by synthesizing nanoprobes through the incubation of NPs with A11 at concentrations of 100, 300, 600, and 900 nM, followed by the
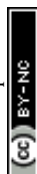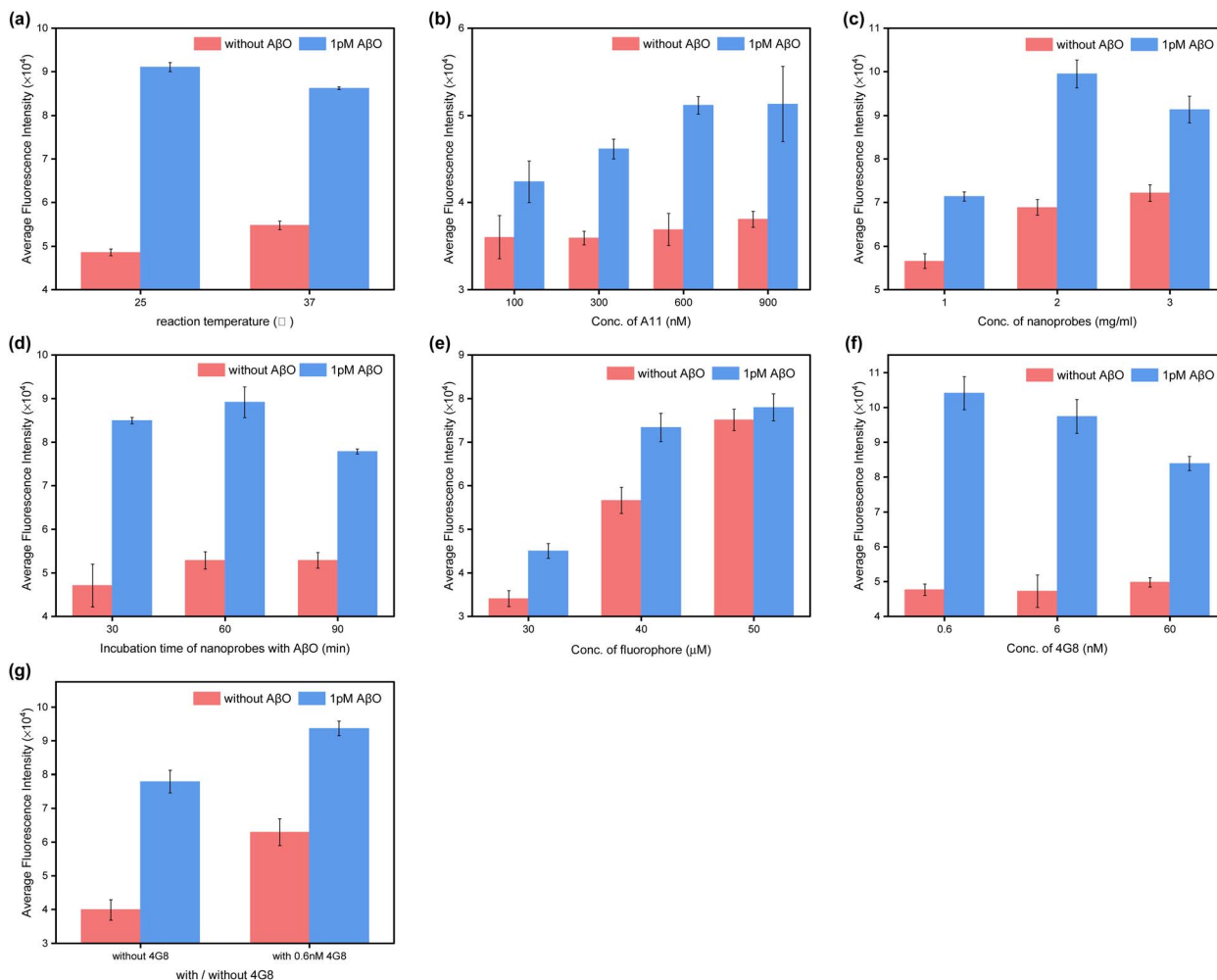
Fig. 3 Optimization of the conditions for the nanosensor. (a) Reaction temperature, (b) concentration of A11 polyclonal antibody, (c) concentration of A11-conjugated nanoprobes, (d) incubation period of nanoprobes with AβO, (e) concentration of O-SLM, (f) concentration of secondary antibody (4G8) and (g) with or without 4G8. Error bars, standard error of the mean; $n = 3$.

incubation with an equivalent concentration of AβO. A significant increase in fluorescence intensity, compared to conditions without the target, indicates enhanced efficiency of the nanoprobes in capturing the target. Striking an equilibrium between antibody coverage and nanoprobe capturing efficiency is essential. Fig. 3b illustrates that an A11 concentration of 600 nM was optimal for synthesizing efficient nanoprobes. Higher concentrations of A11 may result in an excess of antibodies on the surface of the NPs, which may decrease target capture efficiency by disrupting the antibody-antigen recognition process. Moreover, excessive amounts of the capture antibody could lead to increase in background fluorescence in the absence of targets.

An optimal concentration of nanoprobes is also necessary to ensure sufficient reaction platforms available for the capture of protein targets but prevent the aggregation of magnetic immunocomplexes. As illustrated in Fig. 3c, a concentration of 2 mg mL^{-1} of nanoprobes is optimal, resulting in the greatest fluorescence enhancement. In addition, the duration of incubation between the nanoprobes and the analytes plays a significant role in the assay's detection performance. Fig. 3d indicates

that incubating nanoprobes with AβO for 60 min yields the highest fluorescence enhancement. If the incubation time is too short, it may lead to not fully capturing free targets, while prolonged incubation could compromise the activity of capture antibody.

In general, higher concentrations of the fluorophore lead to increased fluorescence intensity. As illustrated in Fig. 3e, the immunocomplexes were labeled with O-SLM concentrations of 30, 40, and 50 μM, respectively, resulting in a rise in fluorescence intensity alongside the increasing O-SLM concentration. However, higher concentrations of O-SLM can increase background noise, potentially negatively impacting the sensor's sensitivity. Consequently, 40 μM of O-SLM was selected for labeling.

In light of the widespread application of secondary antibodies in various immunoassays, we explored the potential benefits of including a secondary antibody in our assay. Initially, detection antibody (4G8) concentrations of 0.6, 6, and 60 nM were tested. Fig. 3f shows that 0.6 nM of 4G8 produced the strongest signal enhancement. However, a comparison between the group without 4G8 and the group containing

0.6 nM of 4G8 revealed that the absence of the secondary antibody resulted in greater fluorescence enhancement (Fig. 3g). This may be attributed to the ineffectiveness of 4G8 in activating the fluorophore while simultaneously consuming the fluorophore and obstructing the binding of AβO with O-SLM. Therefore, the addition of a secondary antibody was omitted from our assay to streamline the detection process.

3.3 Performance of the immunoassay

To substantiate the performance of the developed assay, the sensitivity, selectivity and accuracy of the methodology were assessed. Fig. 4a elucidates the correlation between the fluorescence intensity and the concentration of AβO, delineating a linear relationship within the range of 0–750 fM, accompanied by a robust coefficient of determination ($R^2 = 0.9977$).
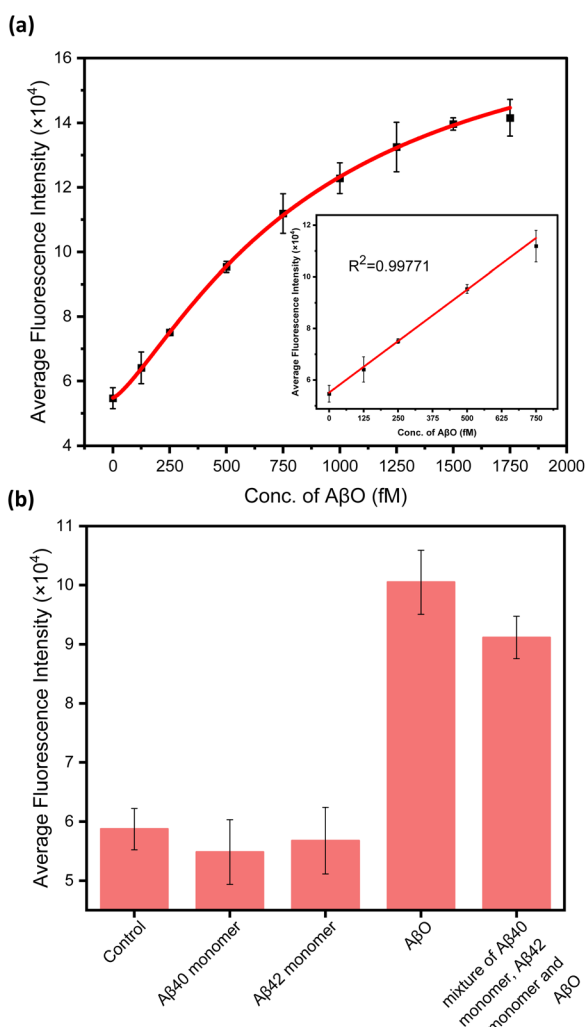

(a)

(b)

Table 1 Recoveries of AβO in diluted human serum samples

Spiked/fM	Measured/fM	Recovery/%	RSD/%
0	199 ± 35	—	—
100	308 ± 11	109 ± 11.3	3.7
200	395 ± 29	97.9 ± 14.3	7.3
400	565 ± 60	91.5 ± 15.0	10.6

Remarkably, this assay has a detection limit as low as 25 fM (LoD = $3.3\sigma/S$, with S being the slope of the calibration curve and σ the standard deviation of the response), which surpasses the sensitivity of the commercial Human Amyloid beta (Aggregated) ELISA Kit (KHB3491 from Invitrogen) by a factor of 7. The specificity of the nanoprobes significantly impacts the precision of the assay, given the diversity of protein types present in human serum, particularly the various forms of amyloid-β proteins that share common epitopes. The Aβ40 monomer, Aβ42 monomer, and aggregated Aβ were analyzed within the developed assay. As demonstrated in Fig. 4b, the fluorescence intensity exhibited only minor changes for the Aβ40 and Aβ42 monomers, while a substantial increase was observed for the AβO and the mixture of the three components. This outcome confirms the assay's specificity for the aggregated form of Aβ, in contrast to the non-aggregated forms. The assay's accuracy was assessed utilizing the standard addition approach. The recoveries of AβO in diluted human serum samples exceeded 90% with relative standard deviation (RSD) values less than 10.6% (Table 1), thereby highlighting the feasibility and reliability of the assay for the analysis of real samples.

3.4 Quantification of AβO in human serum samples

The assay was utilized to measure the serum AβO levels in three neurologically healthy donors (HC #8346, #8353, and #8357) and three AD patients (AD #176886, #230427, and #204262), employing the calibration curve method. The AβO concentrations obtained for each sample are presented in Table 2. As illustrated in Fig. 5, derived from the results in Table 2, the serum AβO concentration in healthy controls is approximately twofold lower than that observed in individuals with AD. This disparity underscores the assay's ability to differentiate between AD patients and individuals without neurological impairment based on serum AβO levels, thereby suggesting its potential utility for AD screening in a clinical setting.

Fig. 4 (a) Fluorescence intensity dependence on concentration of AβO. The inset illustrates the corresponding linear relationship within the 0–750 fM range. Error bars, standard error of the mean; $n = 3$. (b) Selectivity of the nanosensor. The nanoprobes were incubated with 500 fM of Aβ40 monomer, 500 fM of Aβ42 monomer, 500 fM of AβO and a mixture of all three species (500 fM Aβ40 monomer + 500 fM Aβ42 monomer + 500 fM AβO), respectively. Error bars, standard error of the mean; $n = 3$.

Table 2 Concentration of AβO in serum samples from AD patients and healthy controls

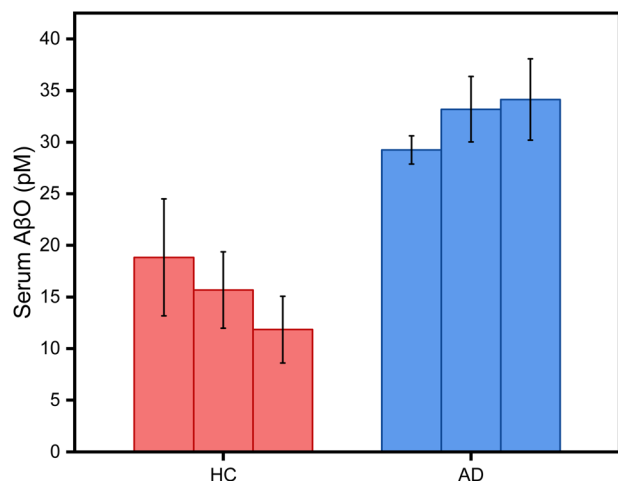| Sample		Measured (fM)	Calculated in serum (pM)	RSD (%)
	#176886	292 ± 14	29.2 ± 1.4	4.7
AD	#230427	332 ± 32	33.2 ± 3.2	9.5
	#204262	341 ± 39	34.1 ± 3.9	11.5
	#8346	188 ± 57	18.8 ± 5.7	30.0
HC	#8353	157 ± 37	15.7 ± 3.7	23.6
	#8357	118 ± 32	11.8 ± 3.2	27.3

Fig. 5 Quantification of AβO in serum samples from healthy controls and AD patients.

4. Conclusions

In this study, we developed a magnetic nanoplatform-based ultrasensitive diagnostic assay for AβO detection, showcasing the assay's versatility and efficacy in early AD diagnosis. The platform's adaptability is illustrated through the incorporation of a specific capture antibody, A11, and the introduction of the tailor-made fluorophore, O-SLM, for enhanced signal amplification. This dual mechanism, combined with magnetic separation, achieves exceptional sensitivity, with detection limits as low as 25 fM—nearly tenfold greater than those of commercial ELISA kits. Notably, our assay requires minimal sample volumes and simplifies the protocol by omitting detection antibodies. The ability to differentiate AD patients from healthy individuals through serum AβO quantification highlights the potential of this magnetic nanoplatform as a cost-effective tool for clinical screening. Furthermore, by expanding the application of this ultrasensitive assay to various biomarkers, such as Aβ42, Tau and neurofilament light (NfL), we aim to enhance the accuracy and reliability of AD diagnoses through comprehensive biomarker profiling. This advancement not only improves diagnostic capabilities but also emphasizes the critical importance of early intervention in AD, which is essential for optimizing treatment outcomes. As we continue to refine and validate this technology, it holds significant promise for impacting clinical practice and improving patient care in managing Alzheimer's disease.

Data availability

The data supporting this article have been included as part of the ESI.†

Conflicts of interest

The authors have no competing interests to declare that are relevant to the content of this article.

References

1 *Alzheimer's Dementia*, 2024, **20**, pp. 3708–3821, DOI: **10.1002/alz.13809**.

2 A. s. D. International, *World Alzheimer Report 2024: Global Changes in Attitudes to Dementia.*, Alzheimer's Disease International, London, England, 2024.

3 Y. Zhang, H. Chen, R. Li, K. Sterling and W. Song, *Signal Transduction Targeted Ther.*, 2023, **8**, 248.

4 K. L. Viola and W. L. Klein, *Acta Neuropathol.*, 2015, **129**, 183–206.

5 *EBioMedicine*, 2016, **9**, pp. 1–2, DOI: **10.1016/j.ebiom.2016.07.001**.

6 D. J. Selkoe and J. Hardy, *EMBO Mol. Med.*, 2016, **8**, 595–608.

7 E. Karran, M. Mercken and B. D. Strooper, *Nat. Rev. Drug Discovery*, 2011, **10**, 698–712.

8 C. Reitz, *Int. J. Alzheimer's Dis.*, 2012, **2012**, 369808.

9 Y. Kim, J. Kim, M. Son, J. Lee, I. Yeo, K. Y. Choi, H. Kim, B. C. Kim, K. H. Lee and Y. Kim, *Sci. Rep.*, 2022, **12**, 1282.

10 H.-N. Chan, D. Xu, S.-L. Ho, M. S. Wong and H.-W. Li, *Chem. Sci.*, 2017, **8**, 4012–4018.

11 L. Blömeke, F. Rehn, V. Kraemer-Schulien, J. Kutzsche, M. Pils, T. Bujnicki, P. Lewczuk, J. Kornhuber, S. D. Freiesleben, L.-S. Schneider, L. Preis, J. Priller, E. J. Spruth, S. Altenstein, A. Lohse, A. Schneider, K. Fliessbach, J. Wiltfang, N. Hansen, A. Rostamzadeh, E. Düzel, W. Glanz, E. I. Incesoy, M. Butryn, K. Buerger, D. Janowitz, M. Ewers, R. Perneczky, B.-S. Rauchmann, S. Teipel, I. Kilimann, D. Goerss, C. Laske, M. H. Munk, C. Sanzenbacher, A. Spottke, N. Roy-Kluth, M. T. Heneka, F. Brosseron, M. Wagner, S. Wolfsgruber, L. Kleineidam, M. Stark, M. Schmid, F. Jessen, O. Bannach, D. Willbold and O. Peters, *Alzheimer's & Dementia: Diagnosis, Assessment & Disease Monitoring*, 2024, **16**, e12589.

12 M. J. Wang, S. Yi, J.-y. Han, S. Y. Park, J.-W. Jang, I. K. Chun, S. E. Kim, B. S. Lee, G. J. Kim, J. S. Yu, K. Lim, S. M. Kang, Y. H. Park, Y. C. Youn, S. S. A. An and S. Kim, *Alzheimer's Res. Ther.*, 2017, **9**, 98.

13 C. M. Gao, A. Y. Yam, X. Wang, E. Magdangal, C. Salisbury, D. Peretz, R. N. Zuckermann, M. D. Connolly, O. Hansson, L. Minthon, H. Zetterberg, K. Blennow, J. P. Fedynyshyn and S. Allauzen, *PLoS One*, 2011, **5**, e15725.

14 J. An, K. Kim, H. J. Lim, H. Y. Kim, J. Shin, I. Park, I. Cho, H. Y. Kim, S. Kim, C. McLean, K. Y. Choi, Y. Kim, K. H. Lee and J. S. Kim, *Nat. Commun.*, 2024, **15**, 1004.

15 K. L. Viola, M. A. Bicca, A. M. Bebenek, D. L. Kranz, V. Nandwana, E. A. Waters, C. R. Haney, M. Lee, A. Gupta, Z. Brahmbhatt, W. Huang, T.-T. Chang, A. Peck, C. Valdez, V. P. Dravid and W. L. Klein, *Front. Neurosci.*, 2022, **15**, 768646.

16 C. Chen, X. Wang, D. Xu, H. Zhang, H.-N. Chan, Z. Zhan, S. Jia, Q. Song, G. Song, H.-W. Li and M. S. Wong, *J. Mater. Chem. B*, 2023, **11**, 4865–4873.

17 Q. Song, H. Zhang, J. Kong, M. S. Wong and H.-W. Li, *Microchim. Acta*, 2025, **192**, 131.